

A FINITE ELEMENT BASED HETEROGENEOUS MULTISCALE METHOD FOR THE LANDAU-LIFSHITZ EQUATION

LENA LEITENMAIER * AND MURTAZO NAZAROV †

Abstract. We present a Heterogeneous Multiscale Method for the Landau-Lifshitz equation with a highly oscillatory diffusion coefficient, a simple model for a ferromagnetic composite. A finite element macro scheme is combined with a finite difference micro model to approximate the effective equation corresponding to the original problem. This makes it possible to obtain effective solutions to problems with rapid material variations on a small scale, described by $\varepsilon \ll 1$, which would be too expensive to resolve in a conventional simulation.

Keywords. Micromagnetics; Heterogeneous Multiscale Methods; Finite element method

AMS subject classifications. 65M12; 65M60; 78M10

1. Introduction Micromagnetic simulations of ferromagnetic materials provide an important tool in physics and material science. The dynamics of the magnetization $\mathbf{M}^\varepsilon : \Omega \times (0, T] \rightarrow \mathbb{R}^3$ are typically described using the Landau-Lifshitz equation,

$$\partial_t \mathbf{M}^\varepsilon(x, t) = -\mathbf{M}^\varepsilon \times \mathbf{H}^\varepsilon(\mathbf{M}^\varepsilon) - \alpha \mathbf{M}^\varepsilon \times (\mathbf{M}^\varepsilon \times \mathbf{H}^\varepsilon(\mathbf{M}^\varepsilon)), \quad x \in \Omega, t > 0, \quad (1.1a)$$

$$\mathbf{M}^\varepsilon(x, 0) = \mathbf{M}_{\text{init}}(x), \quad x \in \Omega, t = 0 \quad (1.1b)$$

$$\nabla \mathbf{M}^\varepsilon \cdot \mathbf{n} = 0, \quad x \in \partial\Omega, t > 0, \quad (1.1c)$$

where α is a material dependent parameter determining the strength of damping and the initial data \mathbf{M}_{init} is such that $|\mathbf{M}_{\text{init}}| = 1$ throughout Ω . The vector \mathbf{n} is the normal to the boundary $\partial\Omega$. Moreover, \mathbf{H}^ε denotes the effective field affecting the magnetization. In this paper, we consider the case of a ferromagnetic composite. A simplified model for this is to introduce a material coefficient a^ε describing the variations in the material, which are on a scale characterized by the parameter $\varepsilon \ll 1$. This type of description has been used in several approaches recently, for example in [5, 6, 12, 24]. With this model, the effective field \mathbf{H}^ε we consider is

$$\mathbf{H}^\varepsilon(\mathbf{M}^\varepsilon) := \nabla \cdot (a^\varepsilon \nabla \mathbf{M}^\varepsilon) + \mathbf{H}_{\text{low}}(\mathbf{M}^\varepsilon),$$

where the first term is due to the exchange interaction between magnetic moments in the material, influenced by the material coefficient, while \mathbf{H}_{low} represents lower order terms, in particular external field, anisotropy and the so-called demagnetization field,

$$\mathbf{H}_{\text{low}}(\mathbf{M}^\varepsilon) = \mathbf{H}_{\text{ext}} + \mathbf{H}_{\text{ani}}(\mathbf{M}^\varepsilon) + \mathbf{H}_{\text{dem}}(\mathbf{M}^\varepsilon).$$

For small values of ε , direct numerical simulation of (1.1) is infeasible since the computational cost becomes too high when resolving the ε -scale. We therefore use the framework of Heterogeneous Multiscale Methods (HMM) [1, 13], which makes it possible to numerically obtain an approximation to the effective solution to the problem. The idea with this framework is to combine a coarse scale macro model, involving a missing quantity that encodes the effect of the fast variations, with a micro model that resolves the fine scale. The micro model is only solved on a small domain in time and space, keeping the

*Department of Mathematics, KTH, Royal Institute of Technology, Stockholm, Sweden, (lenalei@kth.se).

†Division of Scientific Computing, Department of Information Technology, Uppsala University, Sweden (murtazo.nazarov@it.uu.se).

computational cost independent of the scale of the fast variations. The solution to the micro model is then used to approximate the unknown quantity required to complete the macro model.

Several ways to set up HMM for a periodic version of (1.1) are discussed in [20]. A finite difference based implementation of one of these approaches, the so-called field model, is studied in [19]. In this article, we focus on a variation of the so-called flux model and investigate how to combine a finite element macro scheme with a finite difference discretized micro model. This makes it possible to use the approach for more general geometries and gives a high flexibility. Additionally, in contrast to [19], the effective field \mathbf{H}^ε considered in this paper is more general and contains not only the exchange term but also applied field and demagnetization.

This article is structured as follows. We first introduce useful notation and give a definition of the finite element spaces used in Section 2. In Section 3, the HMM approach in general as well as the considered HMM macro and micro model and their numerical solution are described. Related error estimates are given and illustrated with an example. Finally, in Section 4, numerical examples are given to demonstrate the properties of the scheme.

2. Preliminaries

Throughout this article, we consider a domain $\Omega \subset \mathbb{R}^d$, where $d=2$ or 3 . For numerical examples, we use $d=2$. We let $\nabla \mathbf{m}$ denote the Jacobian of $\mathbf{m} \in \mathbb{R}^3$,

$$\nabla \mathbf{m} = [\partial_{x_1} \mathbf{m} \cdots \partial_{x_d} \mathbf{m}].$$

Furthermore, we use the colon-operator to denote the column-wise scalar product of two matrices. Consider matrices $\mathbf{B}, \mathbf{C} \in \mathbb{R}^{3 \times d}$ with columns $\mathbf{b}_j, \mathbf{c}_j \in \mathbb{R}^3$, respectively, then

$$\mathbf{B} : \mathbf{C} = \sum_{j=1}^d \mathbf{b}_j \cdot \mathbf{c}_j.$$

In general, we use the convention that scalar and cross product between a vector and a matrix are done column-wise, and that scalar differential operators are applied element-wise to vector-valued functions. Furthermore, the divergence operator is applied row-wise to a matrix-valued function in order to have consistency with the scalar case in the sense that

$$\nabla \cdot (\nabla \mathbf{m}) = \Delta \mathbf{m}.$$

For the finite element discretization, we introduce an affine mesh \mathcal{T}_h which is a subdivision of Ω into disjoint elements K such that

$$\overline{\Omega} = \bigcup_{K \in \mathcal{T}_h} \overline{K},$$

where $\overline{\Omega}$ and \overline{K} denote the closures of Ω and K , respectively. We consider a family of shape-regular meshes, $\{\mathcal{T}_h\}_{h>0}$, such that each mesh is conforming. The shortest edge in a given triangulation is denoted H_{\min} .

Throughout this paper, we consider Lagrange finite elements and denote the set of nodes $\{N_1, \dots, N_J\} =: \mathcal{N}_h$. The associated piecewise linear scalar nodal basis functions are $\{\phi_j(x)\}_{j=1}^J$, defined such that $\phi_j(x_i) = \delta_{ji}$ for any $i, j \leq J$. Moreover, let χ_K be indicator functions for $K \in \mathcal{T}_h$. Then the space of piecewise linear vector-valued functions

is given by

$$V_h := \{\mathbf{v}_h \in \mathcal{C}^0(\bar{\Omega}; \mathbb{R}^3) \mid \mathbf{v}_h(x) = \sum_{j=1}^J \mathbf{v}_j \phi_j(x), \text{ where } \mathbf{v}_j \in \mathbb{R}^3\}, \quad (2.1)$$

and the space of piecewise constant vector-valued functions is

$$W_h := \{\mathbf{w}_h \mid \mathbf{w}_h(x) = \sum_{K \in \mathcal{T}_h} \mathbf{w}_K \chi_K, \text{ where } \mathbf{w}_K \in \mathbb{R}^3\}. \quad (2.2)$$

We define the interpolation operator $\mathcal{I}_h : \mathcal{C}^0(\Omega; \mathbb{R}^3) \rightarrow V_h$ such that

$$\mathcal{I}_h(\mathbf{m}) := \sum_{j=1}^J \mathbf{m}_j \phi_j(x), \quad \text{where } \mathbf{m}_j := \mathbf{m}(N_j).$$

Note that the Landau-Lifshitz equation (1.1) is length preserving, due to its cross product structure it holds that

$$\partial_t |\mathbf{M}^\varepsilon|^2 = 2\mathbf{M}^\varepsilon \cdot \partial \mathbf{M}^\varepsilon = 0. \quad (2.3)$$

Hence $|\mathbf{M}_{\text{init}}| = 1$ implies that $|\mathbf{M}^\varepsilon(x, t)| = 1$ for all $x \in \Omega$ and $0 \leq t \leq T$. To accommodate this normalization constraint in the finite element solution, we introduce the solution space

$$M_h := \{\mathbf{m}_h \in V_h \mid \mathbf{m}_h(x) = \sum_{j=1}^J \mathbf{m}_j \phi_j(x) \text{ with } |\mathbf{m}_j| = 1\}. \quad (2.4)$$

To make it easier to distinguish between solutions to the HMM micro and macro model, we in general use capitals, for example $\mathbf{M}, \mathbf{M}^\varepsilon$, to refer to solutions on the whole domain Ω . To denote solutions on micro domains, we use lowercase letters, such as \mathbf{m}^ε .

3. Heterogeneous Multiscale Methods

The framework of Heterogeneous Multiscale Methods (HMM) was first introduced by Engquist and E in [13]. The goal with the approach is to achieve numerical homogenization for multiscale problems with scale separation. To accomplish this, one combines a macro and micro model in such a way that the relevant influence of the fast variations in the problem is captured in the micro problem and encoded by an effective quantity, that can then be used to solve the macro scheme on a rather coarse discretization. For a wide range of applications, HMM has been shown to be an efficient way to obtain effective solutions to multiscale problems, as for example described in [1, 14]. Note that due to the fact that an effective solution is approximated by HMM, some error compared to a (numerical) solution to the original problem is introduced. The size of this homogenization error is typically determined by the scale of the fast variations, which are not included in the HMM macro solution. In [18], it was proved that for strong solutions to (1.1) in a periodic setting and corresponding effective solutions, this error is $\mathcal{O}(\varepsilon)$.

3.1. HMM for the Landau-Lifshitz equation

To set up a HMM scheme for the Landau-Lifshitz problem (1.1), consider first the case of a periodic material coefficient, $a^\varepsilon(x) = a(x/\varepsilon)$, where we assume that $a(y) \in \mathcal{C}^\infty(\Omega)$ is bounded by positive constants a_{\min} and a_{\max} , $0 < a_{\min} \leq a(y) \leq a_{\max}$ for all $y \in$

Ω . As we moreover have that the initial data for (1.1), \mathbf{M}_{init} , is such that $|\mathbf{M}_{\text{init}}(x)| = 1$ for all $x \in \Omega$, independent of the material coefficient, we conclude based on [18] that the homogenized problem corresponding to (1.1) is to find $\mathbf{M}_0 : \Omega \times [0, T] \rightarrow \mathbb{R}^3$ such that for $x \in \Omega$ and $0 \leq t \leq T$,

$$\partial_t \mathbf{M}_0(x, t) = -\mathbf{M}_0 \times [\nabla \cdot (\nabla \mathbf{M}_0 \mathbf{A}^H) + \mathbf{H}_{\text{low}}^{\text{hom}}(\mathbf{M}_0)] \quad (3.1a)$$

$$- \alpha \mathbf{M}_0 \times [\mathbf{M}_0 \times (\nabla \cdot (\nabla \mathbf{M}_0 \mathbf{A}^H) + \mathbf{H}_{\text{low}}^{\text{hom}}(\mathbf{M}_0))], \quad (3.1b)$$

$$\mathbf{M}_0(x, 0) = \mathbf{M}_{\text{init}}(x), \quad (3.1b)$$

$$(\nabla \mathbf{M}_0 \mathbf{A}^H) \cdot \mathbf{n} = 0 \quad \text{on } \partial\Omega. \quad (3.1c)$$

The initial data for (3.1) is the same as for (1.1) and $\mathbf{H}_{\text{low}}^{\text{hom}}$ denotes a homogenized version of the lower order field terms. The homogenized coefficient matrix \mathbf{A}^H for the periodic case is the same as for standard elliptic homogenization problems and can be computed by solving

$$\mathbf{A}^H = \int_{[0,1]^d} a(y) (\mathbf{I} + (\nabla_y \chi(y))^T) dy, \quad (3.2)$$

where \mathbf{I} denotes the $d \times d$ identity matrix and χ solves the so-called cell problem

$$\nabla \cdot (a(y) \nabla \chi(y)) = -\nabla_y a(y).$$

REMARK 3.1. *In the rest of this article, we do not consider problems including anisotropy effects. We moreover assume that the variations in the material primarily affect the exchange term, since this is a very short range interaction. The demagnetization, in contrast, is a long range effect. The applied field is in general independent of the magnetization itself. We hence choose in the following to use the approximation*

$$\mathbf{H}_{\text{low}}^{\text{hom}}(\mathbf{M}) \approx \mathbf{H}_L(\mathbf{M}) := \mathbf{H}_{\text{ext}} + \mathbf{H}_{\text{dem}}(\mathbf{M}),$$

which is included in the HMM macro model only. Neglecting changes in the so-called saturation magnetization between the materials, this approximation matches with the results in [5, 6].

Since the homogenized matrix \mathbf{A}^H is symmetric, we have the identity

$$\mathbf{M}_0 \times \nabla \cdot (\nabla \mathbf{M}_0 \mathbf{A}^H) = \nabla \cdot (\mathbf{M}_0 \times (\nabla \mathbf{M}_0 \mathbf{A}^H)),$$

and by the vector triple product identity together with the fact that $|\mathbf{M}_0| = 1$, it follows that

$$-\mathbf{M}_0 \times [\mathbf{M}_0 \times \nabla \cdot (\nabla \mathbf{M}_0 \mathbf{A}^H)] = \nabla \cdot (\nabla \mathbf{M}_0 \mathbf{A}^H) + (\nabla \mathbf{M}_0 : (\nabla \mathbf{M}_0 \mathbf{A}^H)) \mathbf{M}_0.$$

Hence, (3.1a) can be rewritten as

$$\begin{aligned} \partial_t \mathbf{M}_0 = & -\nabla \cdot (\mathbf{M}_0 \times (\nabla \mathbf{M}_0 \mathbf{A}^H)) + \alpha [\nabla \cdot (\nabla \mathbf{M}_0 \mathbf{A}^H) + (\nabla \mathbf{M}_0 : (\nabla \mathbf{M}_0 \mathbf{A}^H)) \mathbf{M}_0] \\ & - \mathbf{M}_0 \times (\mathbf{H}_L(\mathbf{M}_0) + \alpha \mathbf{M}_0 \times \mathbf{H}_L(\mathbf{M}_0)). \end{aligned} \quad (3.3)$$

Taking (3.3) as an inspiration, we deduce that a possible HMM macro model for the problem (1.1) is to find $\mathbf{M}(x, t)$ such that for $x \in \Omega$ and $0 \leq t \leq T$,

$$\partial_t \mathbf{M} = -\nabla \cdot (\mathbf{M} \times \mathbf{F}) + \alpha [\nabla \cdot \mathbf{F} + (\nabla \mathbf{M} : \mathbf{F}) \mathbf{M}] - \mathbf{M} \times [\mathbf{H}_L(\mathbf{M}) + \alpha \mathbf{M} \times \mathbf{H}_L(\mathbf{M})], \quad (3.4a)$$

$$\mathbf{M}(x, 0) = \mathbf{M}_{\text{init}}(x), \quad (3.4b)$$

$$\mathbf{F} \cdot \mathbf{n} = 0 \quad \text{on } \partial\Omega, \quad (3.4c)$$

where the flux $\mathbf{F}(\mathbf{M}, x)$ is unknown and has to be approximated at each discrete point in time t^k where it is needed in a numerical scheme. In case of a periodic material coefficient, $\mathbf{F}(\mathbf{M}, x) \approx \nabla \mathbf{M} \mathbf{A}^H$.

The approximation of \mathbf{F} at a point $x \in \Omega$ is based on the solution \mathbf{m}^ε to the micro problem

$$\partial_t \mathbf{m}^\varepsilon(\xi, \tau) = -\mathbf{m}^\varepsilon \times \nabla \cdot (a^\varepsilon \nabla \mathbf{m}^\varepsilon) - \alpha \mathbf{m}^\varepsilon \times [\mathbf{m}^\varepsilon \times \nabla \cdot (a^\varepsilon \nabla \mathbf{m}^\varepsilon)], \quad (3.5a)$$

$$\mathbf{m}^\varepsilon(\xi, 0) = \mathbf{m}_{\text{init}}(\xi) := \mathbf{M}^k(x + \xi), \quad (3.5b)$$

for $\xi \in \Omega_{\text{mic}}$ and $0 \leq \tau \leq \eta$, where $\eta \sim \varepsilon^2$ and the micro domain is $\Omega_{\text{mic}} = [-\mu', \mu']^d$ with $\mu' \sim \varepsilon$. This implies that the size of the micro domain and time interval is chosen proportional to the scale of the fast variations in the problem [18]. The macro and micro problem are coupled via the initial data to the micro problem, which is set according to the current macro solution $\mathbf{M}^k(x) \approx \mathbf{M}(x, t^k)$ at a given discrete point in time t^k . The solution of the micro problem is described in more detail in Section 3.3.

REMARK 3.2. *Note that in the micro problem (3.5), only the exchange contribution to the effective field is considered. We choose this model based on the considerations given in remark 3.1, and due to the fact that the micro problem only is solved on a small, local domain and for a short time interval. Hence we suppose that strong short-range exchange forces dominate all other forces here. An alternative approach would be to include the lower order field terms in the micro model as well. However, this would result in an increased computational cost as in particular the computation of the long-range demagnetization term is rather computationally expensive [3].*

Once the micro problem is solved, the quantity $a^\varepsilon \nabla \mathbf{m}^\varepsilon$ is averaged in space and time to approximate $\mathbf{F}(\mathbf{M}^k)$. To reduce the approximation error introduced in this process, we use smooth averaging kernels k from the space of kernels $\mathbb{K}^{p,q}$, see [9, 16]. This space of smoothing kernels is defined such that $k \in \mathbb{K}^{p,q}$ given that

$$\int_{-1}^1 k(x) x^r dx = \begin{cases} 1, & r = 0, \\ 0, & 1 \leq r \leq p, \end{cases}$$

and additionally,

$$k \in C_c^q(\mathbb{R}) \text{ with } \text{supp}(k) = [-1, 1], \quad k^{(q+1)} \in BV(\mathbb{R}).$$

Moreover, in [20] the subspace $\mathbb{K}_0^{p,q} \subset \mathbb{K}^{p,q}$ is defined such

$$\mathbb{K}_0^{p,q} := \{k \in \mathbb{K}^{p,q} \mid k(x) = 0 \text{ for } x \leq 0\}.$$

Following the conventions in the field, we use the notation that $k_\mu(x)$ is a scaled version of k ,

$$k_\mu(x) := \frac{1}{\mu} k(x/\mu).$$

In several space dimensions, $d > 1$, we let

$$k(x) := k(x_1) \cdot \dots \cdot k(x_d).$$

Let now $\mathbf{m}^\varepsilon(\xi, \tau)$ be the solution to (3.5) with initial data $\mathbf{m}_{\text{init}}(\xi) = \mathbf{M}^k(x + \xi)$ for $\xi \in \Omega_{\text{mic}}$ and $0 \leq \tau \leq \eta$ with $\eta \sim \varepsilon^2$. Then we define

$$\mathbf{F}(\mathbf{M}^k, x) := \int_{[-\mu, \mu]^d} \int_0^\eta k_\mu(\xi) k_\eta^0(\tau) a^\varepsilon(\xi) \nabla \mathbf{m}^\varepsilon(\xi, \tau) d\tau d\xi, \quad (3.6)$$

where $k \in \mathbb{K}^{p_x, q_x}$ and $k^0 \in \mathbb{K}_0^{p_t, q_t}$, and the averaging parameter μ is chosen such that $\mu \sim \varepsilon$, $\mu \leq \mu'$.

Note that (3.4) to (3.6) is a variation of the so-called flux model in [20]. There estimates for the error introduced when approximating \mathbf{F} are given for the case of a periodic material coefficient and under certain regularity conditions, as well as under the assumption that (3.5) is solved throughout Ω rather than only on Ω_{mic} . Then the approximation error is bounded as given in the following theorem from [20].

THEOREM 3.1. *Assume $a(y) \in \mathcal{C}^\infty(\Omega)$ such that $a_{\min} \leq a(y) \leq a_{\max}$, $0 < \varepsilon < 1$ and $0 < \alpha \leq 1$ and let $\varepsilon^2 < \eta \leq \varepsilon^{3/2}$. Suppose that $\mathbf{m}^\varepsilon(\xi, \tau) \in \mathcal{C}^1([0, \eta]; H^2(\Omega))$ is the exact solution to the micro problem (3.5) for $0 \leq \tau \leq \eta$ and $\xi \in \Omega_{\text{mic}} = [0, 1]^d$ with periodic boundary conditions. Moreover, suppose that there is a constant c independent of ε such that $\|\nabla \mathbf{m}^\varepsilon(\cdot, \tau)\|_{L^\infty} \leq c$ and that the solution to the corresponding homogenized problem is $\mathbf{m}_0 \in \mathcal{C}^\infty(0, \eta, H^\infty(\Omega))$. Consider averaging kernels $k \in \mathbb{K}^{p_x, q_x}$ and $k^0 \in \mathbb{K}_0^{p_t, q_t}$ and let $\varepsilon < \mu < 1$. Then \mathbf{F} as given by (3.6) satisfies*

$$|\mathbf{F} - \nabla \mathbf{m}_{\text{init}}(0) \mathbf{A}^H| =: E_\varepsilon + E_\mu + E_\eta,$$

where

$$E_\varepsilon \leq C\varepsilon, \quad E_\mu \leq C \left(\mu^{p_x+1} + \left(\frac{\varepsilon}{\mu} \right)^{q_x+2} \right) \quad \text{and} \quad E_\eta \leq C \left(\eta^{p_t+1} + \left(\frac{\varepsilon^2}{\eta} \right)^{q_t+1} \right). \quad (3.7)$$

The constant C is independent of ε , μ and η but depends on K , K^0 and α .

3.2. Macro model

The macro problem (3.4) is solved numerically using the finite element method. To obtain a weak formulation for the problem, we multiply (3.4) by a test function $\mathbf{w} \in H^1(\Omega, \mathbb{R}^3)$ and integrate over Ω . This yields the weak problem

$$\begin{aligned} \int_{\Omega} \partial_t \mathbf{M} \cdot \mathbf{w} dx &= \int_{\Omega} (\mathbf{M} \times \mathbf{F}) : \nabla \mathbf{w} dx - \alpha \int_{\Omega} \mathbf{F} : \nabla \mathbf{w} dx + \alpha \int_{\Omega} (\nabla \mathbf{M} : \mathbf{F})(\mathbf{M} \cdot \mathbf{w}) dx \\ &\quad - \int_{\Omega} (\mathbf{M} \times [\mathbf{H}_L(\mathbf{M}) + \alpha \mathbf{M} \times \mathbf{H}_L(\mathbf{M})]) \cdot \mathbf{w} dx, \end{aligned} \quad (3.8)$$

for every test function $\mathbf{w} \in H^1(\Omega, \mathbb{R}^3)$. The boundary terms here vanish due to the given homogeneous Neumann boundary condition, (3.4c).

Note that finite element schemes based on several different weak formulations have been proposed for the Landau-Lifshitz equation. For instance, the schemes in [10] and [4, 7], derived from the so-called Gilbert form of (1.1), an equivalent way to rewrite the equation, are commonly used and can be seen as advantageous with regard to mimicking certain physical properties of the continuous problem. However, in this article we choose the more direct approach in (3.8) since our main goal is to study the combination of micro and macro model and the influence of the flux \mathbf{F} introduced by the HMM approximation. It is possible to introduce the unknown flux \mathbf{F} , approximated from the micro problem, in other weak formulations as well in a similar way.

To solve (3.8) numerically, we adopt an idea from [7] and introduce an unknown variable $\mathbf{v} \approx \partial_t \mathbf{M}$ which replaces $\partial_t \mathbf{M}$ in (3.8). We furthermore discretize in space and time and denote the discretized magnetization at time t^k by $\mathbf{M}_h^k(x) \approx \mathbf{M}(x, t^k)$. For each

discrete time step, the problem then becomes to find $\mathbf{v}_h \in V_h$ such that for all $\mathbf{w}_h \in V_h$,

$$\begin{aligned} \int_{\Omega} \mathbf{v}_h \cdot \mathbf{w}_h dx = & \int_{\Omega} (\mathbf{M}_h^k \times \mathbf{F}_h^k) : \nabla \mathbf{w}_h dx + \alpha \int_{\Omega} (\nabla \mathbf{M}_h^k : \mathbf{F}_h^k) (\mathbf{M}_h^k \cdot \mathbf{w}_h) dx \\ & - \alpha \int_{\Omega} \mathbf{F}_h^k : \nabla \mathbf{w}_h dx - \int_{\Omega} (\mathbf{M}_h^k \times [\mathbf{H}_L(\mathbf{M}_h^k) + \alpha \mathbf{M}_h^k \times \mathbf{H}_L(\mathbf{M}_h^k)]) \cdot \mathbf{w}_h dx, \end{aligned} \quad (3.9)$$

where $\mathbf{M}_h^k \in M_h$ is given and $\mathbf{F}_h^k \in W_h$ is computed by solving the micro problem (3.5) and averaging according to (3.6). Using the notation \mathbf{M}_j^k , $j=1, \dots, J$ for the nodal values of \mathbf{M}_h^k as in (2.4), the time update then is given by

$$\tilde{\mathbf{M}}_j^{k+1} = \mathbf{M}_j^k + \Delta t \mathbf{v}_j, \quad j=1, \dots, J, \quad (3.10a)$$

$$\mathbf{M}_h^{k+1} = \sum_{j=1}^J \mathbf{M}_j^{k+1} \phi_j, \quad \text{where } \mathbf{M}_j^{k+1} = \tilde{\mathbf{M}}_j^{k+1} / |\tilde{\mathbf{M}}_j^{k+1}|, \quad (3.10b)$$

where $\phi_j(x)$ are the piecewise linear basis functions as in the definition of M_h , (2.4). Since (3.9) is a linear problem, it can also be formulated in terms of a bilinear form b and a linear form L . Let

$$b(\mathbf{u}, \mathbf{w}) := \int_{\Omega} \mathbf{u} \cdot \mathbf{w} dx, \quad (3.11)$$

$$\begin{aligned} L(\mathbf{w}; \mathbf{M}_h^k, \mathbf{F}_h^k) := & \int_{\Omega} (\mathbf{M}_h^k \times \mathbf{F}_h^k) : \nabla \mathbf{w} dx + \alpha \int_{\Omega} (\nabla \mathbf{M}_h^k : \mathbf{F}_h^k) (\mathbf{M}_h^k \cdot \mathbf{w}) dx \\ & - \alpha \int_{\Omega} \mathbf{F}_h^k : \nabla \mathbf{w} dx - \int_{\Omega} (\mathbf{M}_h^k \times [\mathbf{H}_L(\mathbf{M}_h^k) + \alpha \mathbf{M}_h^k \times \mathbf{H}_L(\mathbf{M}_h^k)]) \cdot \mathbf{w} dx, \end{aligned} \quad (3.12)$$

then (3.9) is to find $\mathbf{v}_h \in V_h$ such that for all $\mathbf{w}_h \in V_h$,

$$b(\mathbf{v}_h, \mathbf{w}_h) = L(\mathbf{w}_h; \mathbf{M}_h, \mathbf{F}_h).$$

In the literature, for example [4, 10], it is shown that it in many cases is advantageous to use implicit time integration rather than an explicit Euler-like scheme as in (3.10), since with the latter, the time step size Δt has to satisfy a severe time step restriction to obtain stable approximations. However, since the flux \mathbf{F} is unknown and approximated from the micro problem, which implies a very complicated dependence on \mathbf{M} , it can in practice only be treated explicitly in time. To obtain a slightly less harsh time step restriction, we suggest to use a Runge-Kutta based time stepping scheme instead of (3.10). The overall scheme then is described by the following steps:

- Initially, set

$$\mathbf{M}_h^0 = \mathcal{I}_h(\mathbf{M}_{\text{init}}).$$

- Let $\Delta t = T/N$, where the number of time steps N is such that $\Delta t < C \Delta H_{\min}^2$ for a constant $C < 1$, depending on α . For $k=0, \dots, N-1$:
 1. Let $\tilde{\mathbf{M}} = \mathbf{M}_h^k$
 2. For $\ell=1, \dots, 4$:
 - for each face $K \in \mathcal{T}_h$, solve a micro problem (3.5) with initial data given by $\tilde{\mathbf{M}}$ and compute the local value for the flux, \mathbf{F}_K , according to (3.6). Then $\tilde{\mathbf{F}}_h \in W_h$ is

$$\tilde{\mathbf{F}}_h(x) = \sum_{K \in \mathcal{T}_h} \mathbf{F}_K \chi_K,$$

where χ_K are piecewise constant indicator functions as in the definition of W_h , (2.2).

- obtain \mathbf{k}_h^ℓ by solving

$$b(\mathbf{k}_h^\ell, \mathbf{w}_h) = L(\mathbf{w}_h; \tilde{\mathbf{M}}, \tilde{\mathbf{F}}_h) \quad \forall \mathbf{w}_h \in V_h.$$

- set $\tilde{\mathbf{M}} = \mathbf{M}_h^k + c_\ell \Delta t \mathbf{k}^\ell$, where $c_\ell = 1/2$ for $\ell = 1, 2$ and $c_\ell = 1$ for $\ell > 2$ according to the Butcher tableau.

3. Use the stage value functions \mathbf{k}_h^ℓ to obtain $\tilde{\mathbf{M}}^{k+1}$,

$$\tilde{\mathbf{M}}^{k+1} = \mathbf{M}_h^k + \frac{\Delta t}{6} (\mathbf{k}_h^1 + 2\mathbf{k}_h^2 + 2\mathbf{k}_h^3 + \mathbf{k}_h^4).$$

4. Compute \mathbf{M}_h^{k+1} using the normalized nodal values of $\tilde{\mathbf{M}}^{k+1}$,

$$\mathbf{M}_h^{k+1} = \sum_{j=1}^J \mathbf{M}_j^{k+1} \phi_j, \quad \text{where} \quad \mathbf{M}_j^{k+1} = \tilde{\mathbf{M}}_j^{k+1} / |\tilde{\mathbf{M}}_j^{k+1}|.$$

This is what is applied for the numerical experiments in this article. The effect of using a Runge-Kutta rather than Euler based time step update on the time discretization error can for an example problem be seen in Figure 3.1. Both stability and accuracy of the approach improve when using a Runge-Kutta based time step, by far making up for the additional computational effort due to the stage value calculations. However, both approaches are only first order accurate. This is due to the renormalization, step 4 in the description above, see for example also [8]. Note, though, that due to the given time step restriction, $\Delta t < CH_{\min}^2$, we overall still have second order accuracy with respect to the space discretization size.

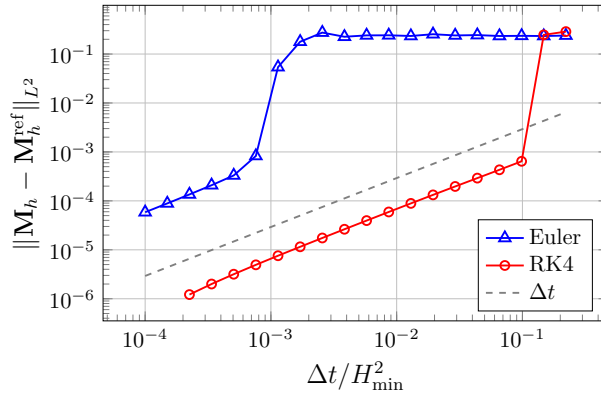


Fig. 3.1: Approximation error with respect to a reference solution when solving (3.1) for an example problem where $\alpha = 0.01$ with the finite element scheme described above for varying Δt . Reference solution $\mathbf{M}_h^{\text{ref}}$ computed with low Δt on the same triangulation as \mathbf{M}_h . The considered example problem is the one described in Section 4.1, where more details are given. Here $H_{\min} = 0.171$ and the selected final time is $T = 1$.

3.3. Micro problem solution and upscaling

In the HMM micro problem around the macro location x and at time t^k , we aim to find $\mathbf{m}^\varepsilon(\xi, \tau)$ such that

$$\partial_t \mathbf{m}^\varepsilon(\xi, \tau) = -\mathbf{m}^\varepsilon \times [\nabla \cdot (a^\varepsilon \nabla \mathbf{m}^\varepsilon) + \alpha \mathbf{m}^\varepsilon \times \nabla \cdot (a^\varepsilon \nabla \mathbf{m}^\varepsilon)], \quad \xi \in \Omega_{\text{mic}}, 0 < \tau \leq \eta, \quad (3.13a)$$

$$\mathbf{m}^\varepsilon(\xi, 0) = \mathbf{m}_{\text{init}}(\xi) := \mathbf{M}^k(x + \xi), \quad \xi \in \Omega_{\text{mic}}, \tau = 0, \quad (3.13b)$$

$$\mathbf{m}^\varepsilon(\xi, t) = \mathbf{m}_{\text{init}}(\xi), \quad \xi \in \partial\Omega_{\text{mic}}, \tau > 0, \quad (3.13c)$$

where the considered final time is $\eta \sim \varepsilon^2$ and the micro problem domain is $\Omega_{\text{mic}} = [-\mu', \mu']^d$ with $\mu' \sim \varepsilon$. We moreover suppose that μ' is such that the whole micro domain Ω_{mic} is inside one triangle of the macro discretization, located around the barycenter. Note that the latter assumption is due to reasons of simplicity and comes naturally for small values of ε . In the following, we focus on the case $d=2$. A schematic overview of the connection between macro domain Ω , micro problem domain Ω_{mic} and averaging domain $[-\mu, \mu]^2$ is given in Figure 3.2.

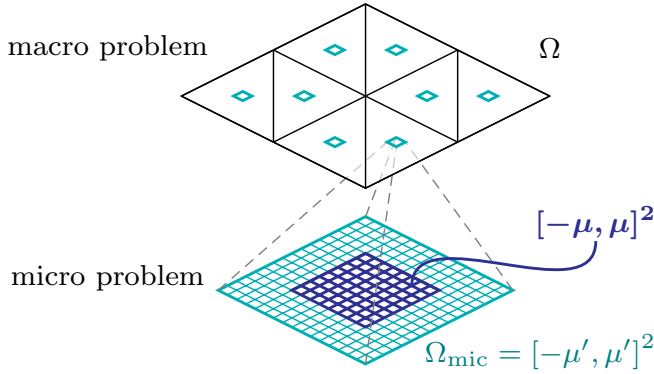


Fig. 3.2: Domains involved in the HMM approach.

The initial data \mathbf{m}_{init} for the micro problem is chosen according to the current macro solution \mathbf{M}_h^k at time t^k in the domain Ω_{mic} . As \mathbf{M}_h^k is a piecewise bilinear function, the same holds for \mathbf{m}_{init} . Note that this implies that \mathbf{m}_{init} is not normalized. As a consequence, an additional error is introduced in the upscaling process. In numerical experiments, this term appears to be $\mathcal{O}(H)$, where H describes the shortest edge of the corresponding macro triangle. In the following, we account for this error by adding an additional term, E_{norm} , to the error estimate as stated in Theorem 3.1. Note that in the periodic case and given a finite element approximation $\mathbf{M}_h \in M_h$ to an (unknown) actual solution \mathbf{M}_{ref} , we know that with the given scheme, it holds that $\mathbf{F}(x, \mathbf{M}_h) \approx \nabla \mathbf{M}_h(x) \mathbf{A}^H$, and that when using piecewise linear finite elements, $\nabla \mathbf{M}_h = \nabla \mathbf{M}_{\text{ref}} + \mathcal{O}(H)$. Hence the additional upscaling error is of the same order as this approximation error.

Furthermore, as stated in (3.13), the micro problem is completed with Dirichlet boundary conditions. These boundary conditions are artificial and cause an additional error, in the following denoted by $E_{\mu'}$. When considering an infinite domain, that is as $\mu' - \mu \rightarrow \infty$, this error term vanishes. In practice, we cannot have an infinitely large computational domain. We instead choose μ' such that $E_{\mu'}$ does not significantly influence the upscaling error but not much larger in order to not increase the computational

cost more than necessary. In general, μ' has to be chosen larger when larger final times η are considered, since with increasing time, the errors caused by the artificial boundary conditions travel further into the domain.

To solve (3.5) numerically, the problem is discretized in space using a second order accurate finite difference scheme, based on a regular grid with mesh size $\Delta\xi = 2\mu'/N_{\text{mic}}$. Let $a_{i,j} := a(-\mu' + i\Delta\xi, -\mu' + j\Delta\xi)$ and $\mathbf{m}_{i,j}(\tau) \approx \mathbf{m}^\varepsilon((-\mu' + i\Delta\xi, -\mu' + j\Delta\xi), \tau)$, for $i, j = 0, \dots, N_{\text{mic}}$. Then the semi-discrete system obtained by discretization of (3.13) in space is

$$\partial_\tau \mathbf{m}_{i,j}(\tau) = \mathbf{f}_{i,j}(\mathbf{m}), \quad \text{for } i, j = 1, \dots, N_{\text{mic}} - 1,$$

where

$$\begin{aligned} \mathbf{f}_{i,j}(\mathbf{m}) &:= -\mathbf{m}_{i,j} \times \mathbf{H}_{i,j}(\mathbf{m}) - \alpha \mathbf{m}_{i,j} \times [\mathbf{m}_{i,j} \times \mathbf{H}_{i,j}(\mathbf{m})], \\ \mathbf{H}_{i,j}(\mathbf{m}) &:= \frac{1}{\Delta\xi^2} \left[a_{i+\frac{1}{2},j} \mathbf{m}_{i+1,j} + a_{i-\frac{1}{2},j} \mathbf{m}_{i-1,j} + a_{i,j+\frac{1}{2}} \mathbf{m}_{i,j+1} + a_{i,j-\frac{1}{2}} \mathbf{m}_{i,j-1} \right. \\ &\quad \left. - (a_{i+\frac{1}{2},j} + a_{i-\frac{1}{2},j} + a_{i,j+\frac{1}{2}} + a_{i,j-\frac{1}{2}}) \mathbf{m}_{i,j} \right]. \end{aligned}$$

At $i=0$, $j=0$, $i=N_{\text{mic}}$ or $j=N_{\text{mic}}$, we have $\mathbf{m}_{i,j} = \mathbf{m}_{\text{init}}(-\mu' + i\Delta\xi, -\mu' + j\Delta\xi)$. For time integration, we use the midpoint extrapolation method (MPE) [25], a second order accurate integrator that is norm preserving without any projections, which makes it suitable for the non-normalized initial data. Let $\mathbf{m}_{i,j}^k \approx \mathbf{m}_{i,j}(\tau_k)$, where $\tau_k = k\Delta\tau$ for $k=0, \dots, M_{\text{mic}}$ and $\Delta\tau = \eta/M_{\text{mic}}$. Then the time integration is described by

$$\mathbf{m}_{i,j}^{k+1} = \mathbf{m}_{i,j}^k - \Delta\tau \frac{\mathbf{m}_{i,j}^{k+1} + \mathbf{m}_{i,j}^k}{2} \times \mathbf{h}_{i,j}^{k+1/2},$$

where

$$\mathbf{h}_{i,j}(\mathbf{m}) := \mathbf{H}_{i,j}(\mathbf{m}) + \mathbf{m}_{i,j} \times \mathbf{H}_{i,j}(\mathbf{m})$$

and $\mathbf{h}^{k+1/2}$ is a second order extrapolation approximating $\mathbf{h}_{i,j}(\frac{1}{2}(\mathbf{m}^k + \mathbf{m}^{k+1}))$,

$$\mathbf{h}_{i,j}^{k+1/2} := \frac{3}{2} \mathbf{h}_{i,j}(\mathbf{m}^k) - \frac{1}{2} \mathbf{h}_{i,j}(\mathbf{m}^{k-1}).$$

Note that with this time stepping scheme, one only obtains stable solutions given that

$$\Delta\tau \leq C \Delta\xi^2, \quad (3.14)$$

for some constant C independent of $\Delta\xi$ but dependent on the damping parameter α . A detailed discussion of a micro problem similar to the one discussed here is given in [19]. As suggested there, also in this paper we use artificial damping in the micro problem and choose $\alpha \approx 1$, which leads to an improved constant in the error estimate in Theorem 3.1 and thus convergence of the approximation errors for shorter final times η . The averaging kernels k and k^0 in (3.6) are chosen such that $p_x = p_t = 3$ and $q_x = q_t = 7$. As we moreover have $\mu \sim \varepsilon$ and $\eta \sim \varepsilon^2$, we can simplify the error estimate for the periodic case given in (3.7), which together with the additional error terms due to the micro problem setup yields

$$|\mathbf{F} - \nabla \mathbf{m}_{\text{init}}(0,0) \mathbf{A}^H| \approx C \left[\varepsilon + \left(\frac{\varepsilon}{\mu} \right)^{q+2} + \left(\frac{\varepsilon^2}{\eta} \right)^{q+1} \right] + E_{\mu'} + E_{\text{norm}} + \mathcal{O}(\Delta\xi^2). \quad (3.15)$$

The last term here, $\mathcal{O}(\Delta\xi^2)$, is due to the discretization error introduced when solving the micro problem numerically as described above.

While the error estimate in Theorem 3.1 is only proved for periodic material coefficients, we find that the upscaling errors still behave according to (3.15) for somewhat more general coefficients. To demonstrate this, and to investigate how the choices of μ, η and μ' influence the approximation error, we consider a numerical example with the locally periodic material coefficient

$$a^\varepsilon(x) = 1.1 + \frac{1}{2} [\sin(2\pi x_1/\varepsilon) + \sin(2\pi x_2/\varepsilon)] \cos(2\pi(x_1 + x_2)). \quad (3.16)$$

The corresponding homogenized matrix at the fixed location $x = (0,0)$ can be determined by freezing the slow variables and computing \mathbf{A}^H according to (3.2). This can be used to obtain a reference solution for one micro problem, given macro data on one triangle with barycenter in $(0,0)$.

To investigate the averaging errors, we then first fix $\varepsilon = 10^{-4}$, and choose μ and μ' such that they do not influence the upscaling error significantly, for this example $\mu = 3\varepsilon$ and $\mu' = 15\varepsilon$. Moreover, we pick $\Delta\xi$ such that the numerical discretization error is small and select $\alpha = 1.5$, which means that we consider a setup with artificial damping. Then the upscaling error is determined by η and H , and the estimate in (3.15) simplifies to

$$|\mathbf{F} - \nabla \mathbf{m}_{\text{init}}(0,0) \mathbf{A}^H| \approx C \left(\frac{\varepsilon^2}{\eta} \right)^{q+1} + E_{\text{norm}}.$$

In Figure 3.3a, the upscaling error for varying η and several choices of macro discretization length H is shown. One can observe that the error decreases rapidly as η increases, until it saturates at a level proportional to H , which corresponds to E_{norm} .

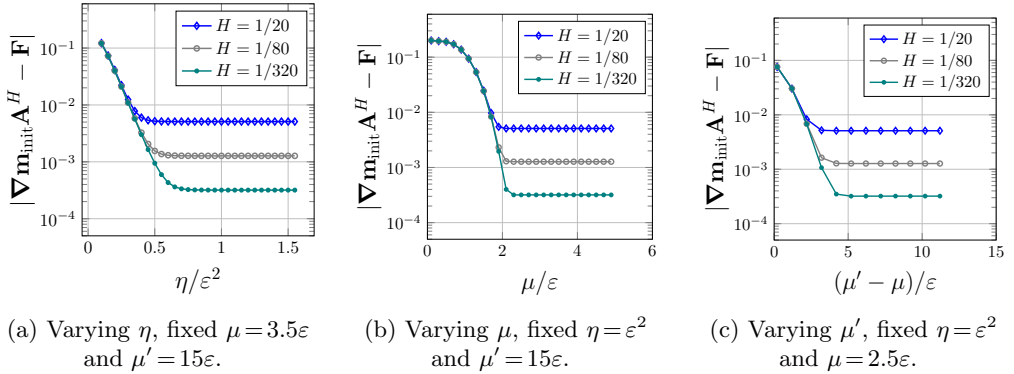


Fig. 3.3: Influence of the micro problem parameters on the upscaling error.

Next, we fix the length of the micro time interval to $\eta = \varepsilon^2$ and vary the length of the spatial averaging domain, μ . All other parameters stay fixed. In this case, the error estimate (3.15) becomes

$$|\mathbf{F} - \nabla \mathbf{m}_{\text{init}}(0,0) \mathbf{A}^H| \approx C \left(\frac{\varepsilon}{\mu} \right)^{q+2} + E_{\text{norm}}. \quad (3.17)$$

The resulting errors are plotted in Figure 3.3b. As shown there, as μ becomes larger than ε , the error decreases rapidly and then, once $\mu \gtrsim 2\varepsilon$, saturates at a level determined by the given value of H , the same as in Figure 3.3a, corresponding to E_{norm} .

Finally, both η and μ are fixed and the micro domain size μ' is varied. In this case, $E_{\mu'}$, for which no explicit formula is known, and again E_{norm} determine the resulting upscaling error, which is shown in Figure 3.3c. Based on this plot, we come to the conclusion that taking $\mu' \approx \mu + 5\varepsilon$ is sufficient to reduce the error introduced by the artificial boundary conditions so that it does not influence the overall error in a significant way.

Further examples of how the upscaling error is influenced by the choice of η , μ and μ' are given in [19] for a similar but slightly different micro problem. We here conclude that choosing η , μ and μ' large enough results in upscaling errors determined only by H . Given a smaller value of H , lower errors can be obtained by selecting the parameters η and as a consequence μ' larger. The optimal value for μ is only affected marginally.

The computational cost per micro problem can be described in terms of the number of points used to resolve the ε scale. Let $P := \varepsilon/\Delta\xi$, then the total number of discretization points for the micro problem is determined by $N_{\text{mic}}^2 = (2\mu'/\Delta\xi)^2 = 4P^2(\mu'/\varepsilon)^2$. Moreover, due to the time step restriction (3.14), the number of time steps per micro problem has to be chosen to be $M_{\text{mic}} = \eta/\Delta\tau = C\eta/\Delta\xi^2 = CP^2(\eta/\varepsilon^2)$. Hence, the overall cost per micro problem is given by

$$\text{cost} \sim CM_{\text{mic}}N_{\text{mic}}^2 \sim CP^4 \left(\frac{\mu'}{\varepsilon}\right)^2 \left(\frac{\eta}{\varepsilon^2}\right). \quad (3.18)$$

As $\mu' \sim \varepsilon$ and $\eta \sim \varepsilon^2$, this shows that the computational cost per micro problem is independent of ε . This makes it possible to apply the HMM approach even for very small values of ε , where the resolution of the fine scale with a conventional approach would result in tremendously high computational cost.

Note, though, that to keep the overall cost down, one should choose μ' and η not larger than necessary and select a relatively low value of P . For the example problems discussed in the next section, $P \approx 10$ provides a reasonable compromise between accuracy and computational cost.

4. Numerical examples

In this section, we give several numerical examples to illustrate the proposed scheme. We mostly focus on periodic material coefficients to be able to provide corresponding homogenized solutions for reference. In the final example, the locally periodic case discussed in Section 3.3 is considered. In all the presented examples, we use homogeneous Neumann boundary conditions as in (3.1), (3.4).

4.1. Circular domain example As a first numerical example, we consider a variation of the problem suggested in [4], with a circular 2D domain $\Omega = B(0,1)$ and initial data

$$\mathbf{M}_{\text{init}}(x) = \left[-\frac{x_2}{r} \sin\left(\frac{\pi r}{2}\right), \frac{x_1}{r} \sin\left(\frac{\pi r}{2}\right), \cos\left(\frac{\pi r}{2}\right) \right]^T, \quad (4.1)$$

where $r = \sqrt{x_1^2 + x_2^2}$. Only the exchange term in the effective field is considered, $\mathbf{H}^\varepsilon = \nabla \cdot (a^\varepsilon \nabla \mathbf{m}^\varepsilon)$, where a^ε is assumed to be a periodic material coefficient,

$$a^\varepsilon(x) := (1.1 + 0.25 \sin(2\pi x_1/\varepsilon))(1.1 + 0.25 \sin(2\pi x_2/\varepsilon)) + 0.7 \cos(2\pi(x_1 - x_2)/\varepsilon). \quad (4.2)$$

The corresponding homogenized coefficient matrix, which is used to solve the related homogenized problem for reference, is

$$\mathbf{A}^H \approx \begin{bmatrix} 1.057 & 0.118 \\ 0.118 & 1.057 \end{bmatrix},$$

which is computed numerically with high accuracy for the simulation. Moreover, the average of the given material coefficient, (4.2), is $a_{\text{avg}} = 1.21$. We include the solution to (1.1) with the material coefficient replaced by its average, a_{avg} , in the example since this can be seen as a naive approach to dealing with the oscillations in the problem. We do not expect this to give the correct solutions. The main reason of including it is to show that the chosen example is relevant in the sense that its solution with the naive coefficient a_{avg} differs significantly from the correct solution.

The implementation of the finite element code for the numerical examples in this article is done using the FEniCS project [21]. For mesh generation, we use gmsh [17]. The initial data to the problem according to (4.1) and a mesh for the domain are shown in Figure 4.1. There the domain is colored according to the x -component of the data and the vectors show the direction of the magnetization. Note that the z -direction is out of plane.

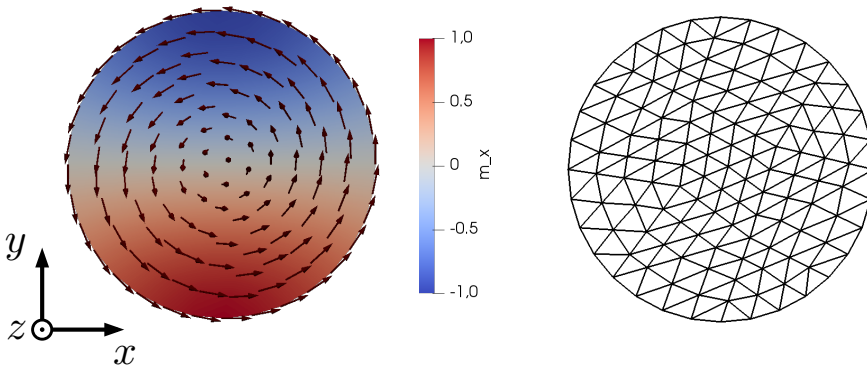


Fig. 4.1: Initial data for the numerical example according to (4.1) and computational mesh for the macro domain.

For the HMM solution of this problem, we use artificial damping and set $\alpha = 1.2$ in the micro problem. We choose $\varepsilon = 10^{-4}$ in the example. Moreover, we consider two different setups of averaging parameters:

- setup 1: $\mu' = 4.8\varepsilon$, $\mu = 2.8\varepsilon$ and $\eta = 0.45\varepsilon^2$, which results in an upscaling error of approximately $0.002 + H$ for the micro problem around $(0,0)$,
- setup 2: $\mu' = 3.25\varepsilon$, $\mu = 2.1\varepsilon$ and $\eta = 0.15\varepsilon^2$, which gives an upscaling error of approximately $0.02 + H$ for the same micro problem.

Consider a final time $T = 1.0$ and the macro discretization using the mesh in Figure 4.1. Then in Figure 4.2 the corresponding solution to the homogenized problem, the HMM solution with the micro parameters set according to setup 1, and the solution when using the average of the material coefficient are shown. One can observe that homogenized and HMM solution agree very well while the averaged-coefficient solution is different.

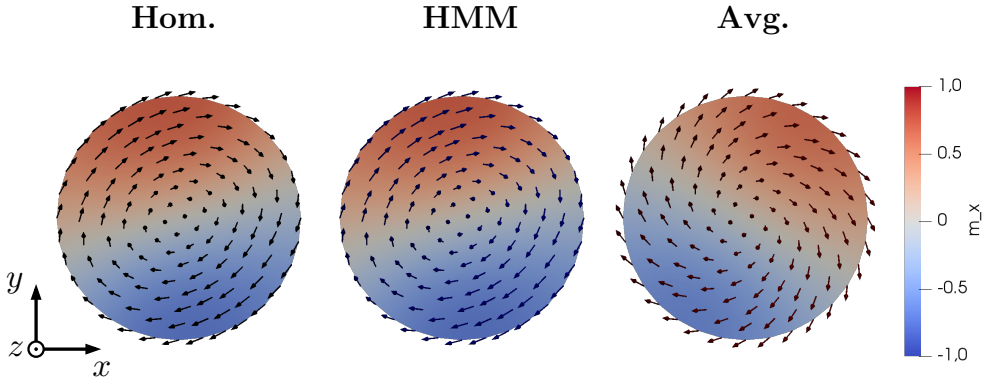


Fig. 4.2: Numerical solution to homogenized problem (left), HMM solution (middle) and average coefficient solution (right) at time $T=1.0$ to (1.1) with material coefficient (4.2), initial data according to (4.1) and $\alpha=0.2$ on the macro scale. Domain colored according to x -component of \mathbf{M} .

Furthermore, in Table 4.1, the L^2 norm of the difference between HMM solution and homogenized solution on a finer grid at time $T=0.5$ are given. With setup 1, corresponding to a sufficiently low upscaling error, we observe second order convergence of the HMM solution towards the reference solution. With setup 2, on the other hand, the errors initially decrease when refining the computational grid but then seem to saturate. This is due to the fact that in this case, the upscaling error is larger and hence affects the HMM solution more. We expect a similar effect to appear also with the first micro parameter setup, but for more refined grids, with lower H_{\min} .

H_{\min}	$\ \mathbf{M} - \mathbf{M}_{\text{ref}}\ _{L^2}$ setup 1	conv. order	$\ \mathbf{M} - \mathbf{M}_{\text{ref}}\ _{L^2}$ setup 2	conv. order
0.684	0.0663		0.0858	
0.342	0.0197	1.75	0.0273	1.65
0.171	0.00557	1.82	0.0129	1.08
0.0855	0.00139	2.00	0.0101	0.353

Table 4.1: Convergence of the HMM solution at time $T=0.5$ with respect to a homogenized reference solution on a fine grid. Same choice of initial data and material coefficient as in Figure 4.2 and again $\alpha=0.2$.

We then furthermore extend the example problem and additionally consider an applied external field,

$$\mathbf{H}_{\text{ex}} = [10, 10, 0]^T,$$

which is turned on at time $T=0.5$. This causes the magnetization vectors to align accordingly, as shown in Figure 4.3.

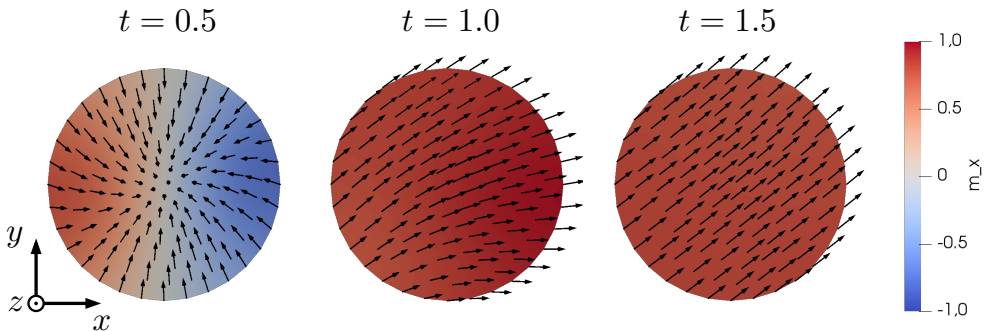


Fig. 4.3: Influence of an external field. Same example as in Figure 4.2 but with $\mathbf{H}_{\text{ex}} = [10, 10, 0]^T$ applied for $t > 0.5$.

4.2. Ring example Inspired by [11], we next consider a ring-shaped domain with outer radius $R_{\text{out}} = 1$ and inner radius $R_{\text{in}} = 0.4$. Initially, the magnetization in the ring is given by

$$\mathbf{M}_{\text{init}}(x) = \left[-\frac{x_2}{r}, \frac{x_1}{r}, 0 \right]^T, \quad (4.3)$$

where again $r = \sqrt{x_1^2 + x_2^2}$, which is close to a stable state, except for a small subsection of the domain where we instead set $\mathbf{M}_{\text{init}} = [1, 0, 0]^T$, a simplified representation of a defect. This is shown in Figure 4.4 at time $t = 0$. For this example problem, we set the damping parameter to $\alpha = 0.02$ (on the macro scale) and use the same material coefficient a^ε as in the previous example, (4.2). Only the exchange-term is considered in the effective field. The micro parameters are selected to be $\eta = 0.3\varepsilon^2$, $\mu = 2.1\varepsilon$ and $\mu' = 4.25$, in between the two setups considered in the previous subsection, and $\varepsilon = 10^{-3}$. Furthermore, artificial damping with $\alpha = 1.2$ is used in the micro problem.

The resulting HMM solution at several points in time is shown in Figure 4.4. Due to the defect, the magnetization throughout the ring is affected and varies as the magnetization vectors strive towards a state of alignment.

Furthermore, for the final time $T = 0.3$, the error between homogenized solution \mathbf{M}_0 and HMM solution as well as between homogenized solution and the solution obtained when using the average of the material coefficient is shown in Figure 4.5. One can observe that despite the coarser choice of micro problem parameters, the HMM solution agrees well with the homogenized solution, while the average coefficient solution shows high errors.

4.3. Landau-state example As a further example, we consider relaxation towards a so-called Landau-state. A domain of length and width 250 nm and thickness 2 nm is given, which in a non-dimensional setting is represented by a 2D unit-square domain. The third dimension, with much smaller extent than the other two, is only considered in the computation of the demagnetization term. A time interval of 1 ns is assumed and the damping parameter is selected as $\alpha = 0.05$. The initial data is set such that the magnetization eventually attains a so-called Landau state,

$$\mathbf{M}_{\text{init}} = \begin{cases} [0, 1, 0]^T & x_1 < 0.5 \\ [0, -1, 0]^T & \text{otherwise.} \end{cases}$$

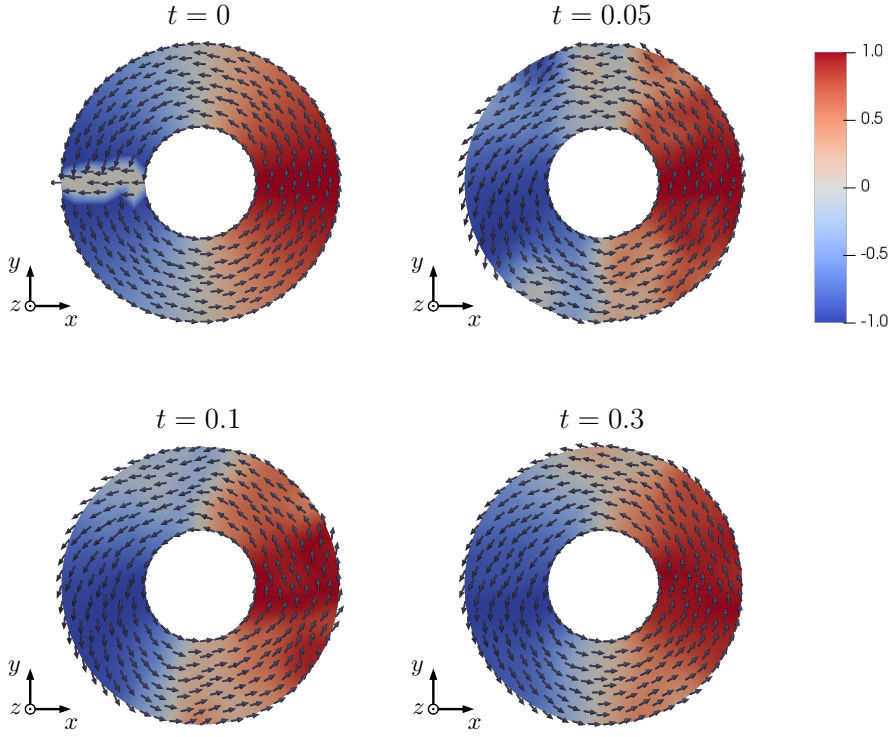


Fig. 4.4: HMM solution to the ring example problem. Domain colored according to y -component of \mathbf{M} .

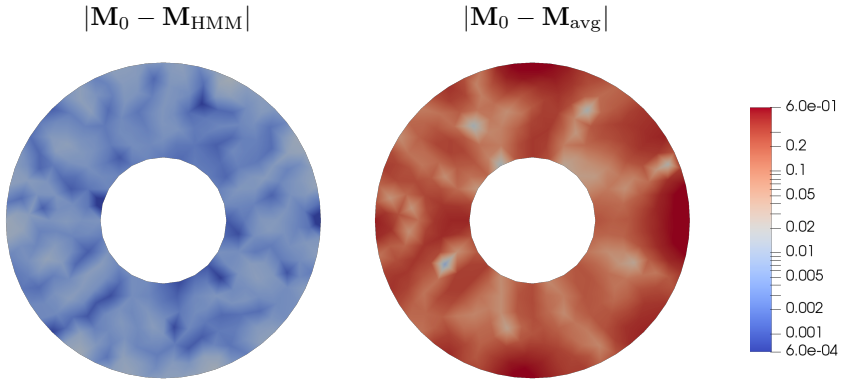


Fig. 4.5: Difference between homogenized solution (for reference) and HMM solution or average coefficient solution, respectively.

The effective field in this example consists of exchange term and demagnetization,

$$\mathbf{H}^\varepsilon = \nabla \cdot (a^\varepsilon \nabla \mathbf{m}^\varepsilon) + \mathbf{H}_{\text{dem}}.$$

In general, the demagnetization field is given by $\mathbf{H}_{\text{dem}} = -\nabla u$, where the scalar potential u solves

$$\Delta u = \begin{cases} \nabla \cdot \mathbf{M} & \text{in } \Omega, \\ 0 & \text{in } \mathbb{R}^3 \setminus \Omega. \end{cases}$$

For reasons of simplicity, the demagnetization term for this example problem is computed using the algorithm proposed in [23], specifically using a C++ implementation along the lines of [2]. This algorithm uses the fact that \mathbf{H}_{dem} can also be expressed as

$$\mathbf{H}_{\text{dem}} = \int_{\Omega} \tilde{\mathbf{N}}(x-y) \mathbf{M}(y) dy, \quad \text{where} \quad \tilde{\mathbf{N}}(x-y) = -\frac{1}{4\pi} \nabla \nabla_y \frac{1}{|x-y|}.$$

For an efficient implementation, the demagnetization tensor $\tilde{\mathbf{N}}$ is pre-computed and the convolution integral is evaluated using the Fast Fourier transform. It is computed on a regular grid in a separate module which is coupled with the finite element solver.

To make it possible to compare to a homogenized solution for reference, we use another periodic material coefficient,

$$a^\varepsilon = \exp[\cos(2\pi(x+y)/\varepsilon) - 0.25 \sin(2\pi x/\varepsilon)].$$

The corresponding homogenized matrix is approximately

$$\mathbf{A}^H = \begin{bmatrix} 1.014 & -0.234 \\ -0.234 & 1.04 \end{bmatrix}.$$

In this example problem, we set $\varepsilon = 10^{-3}$ and select the micro problem parameters to be $\eta = 0.3\varepsilon^2$, $\mu = 2.1\varepsilon$ and $\mu' = 5.5\varepsilon$. For the micro problem, $\alpha = 1.2$. The obtained HMM solution at times corresponding to 0 to 0.5 ns is shown in Figure 4.6.

Moreover, the difference between a corresponding homogenized solution \mathbf{M}_0 and the HMM solution at time corresponding to $t = 0.5$ ns is shown in Figure 4.7. For comparison, also the error between the homogenized solution \mathbf{M}_0 and what is obtained when approximating a^ε by its average a_{avg} , a solution \mathbf{M}_{avg} , is shown. One can observe that the HMM solution agrees considerably better with the homogenized solution than \mathbf{M}_{avg} .

4.4. Modification of μMAG standard problem 4 As a final example, we consider a variation of the μMAG standard problem 4 [22], with a locally periodic material coefficient,

$$a^\varepsilon(x) = 1.1 + \frac{1}{2} [\sin(2\pi x_1/\varepsilon) + \sin(2\pi x_2/\varepsilon)] \cos(2\pi(x_1 + x_2)), \quad (4.4)$$

the same coefficient as in the example in Section 3.3. In the μMAG problem, a thin film domain of length 500 nm, width 125 nm and thickness 3 nm is considered. The dimensional form of the Landau-Lifshitz equation is used, with material parameters similar to permalloy. In this article, we use a corresponding non-dimensionalized, rescaled setup and a 2D domain of length 4 and width 1. The third dimension is again only taken into

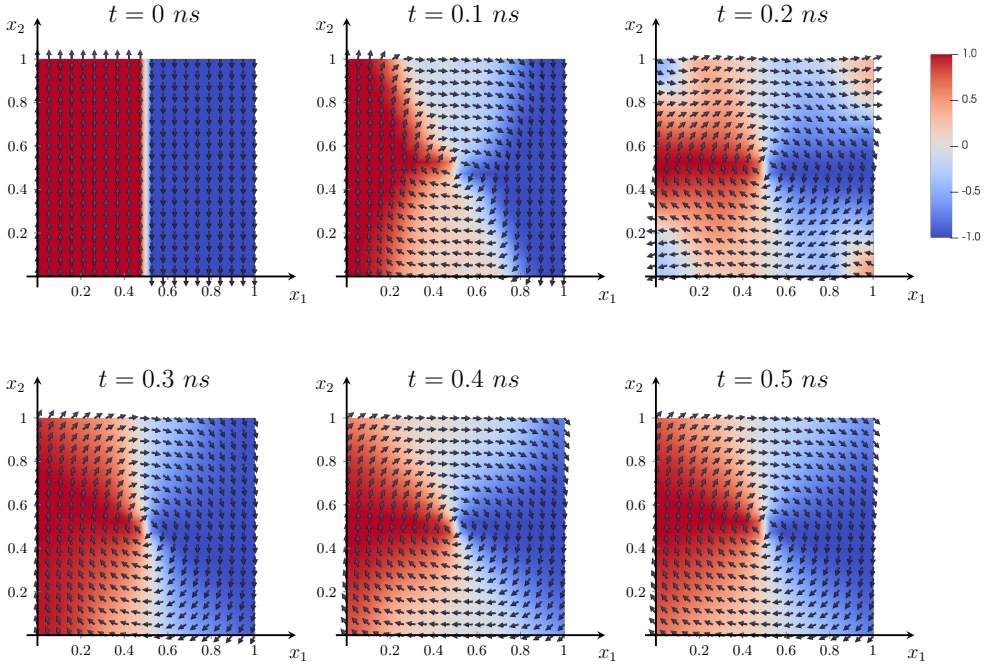


Fig. 4.6: HMM solution to the Landau-state example problem for different points in time. Domain colored according to y -component of the magnetization.

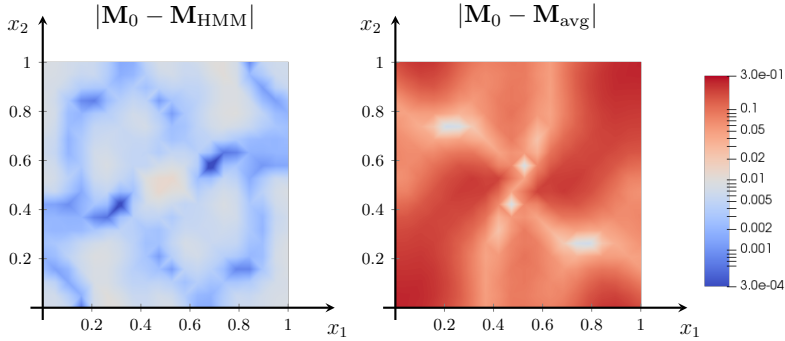


Fig. 4.7: Error in HMM and avg. coefficient solution at time $t = 0.5 ns$

account in the computation of the demagnetization. As initial data for this problem, a so-called equilibrium s-state is used, as shown in Figure 4.8. We obtain this s-state by first setting the magnetization to

$$\mathbf{M}_{\text{init}} = [\cos(\pi x_1/8), \sin(\pi x_1/8), 0]^T, \quad (4.5)$$

and then relaxing until equilibrium is reached. Once the initial s-state is achieved, an external field is applied, corresponding to $[-24.6, 4.3, 0.0]^T / \mu_0 \text{ mT}$, where μ_0 denotes the

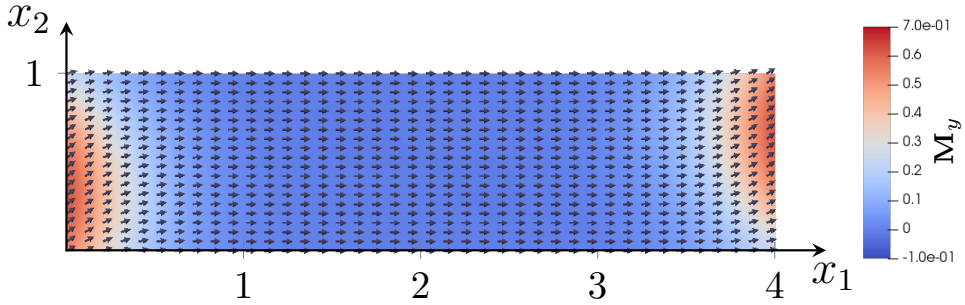


Fig. 4.8: The equilibrium s-state obtained from the initial data (4.5) with material coefficient a^ε given by (4.4), colored according to y -component of \mathbf{M} .

vacuum permeability, $\mu_0 = 4\pi \cdot 10^{-7} \text{ N/A}^2$, in the dimensional problem. The damping parameter is set to $\alpha = 0.02$.

In this final example problem, we consider exchange interaction, applied external field and demagnetization,

$$\mathbf{H}^\varepsilon = \nabla \cdot (a^\varepsilon \nabla \mathbf{m}^\varepsilon) + \mathbf{H}_{\text{ex}} + \mathbf{H}_{\text{dem}}.$$

The demagnetization is computed as described for the previous example.

The HMM micro problem parameters for this example are chosen according to the discussions in Section 3.3, based on Figure 3.3. We use $\alpha = 1.5$ and set $\eta = 0.5\varepsilon^2$, $\mu = 2.1\varepsilon$ and $\mu' = 6.5\varepsilon$, where in this example, $\varepsilon = 10^{-3}$.

The corresponding HMM solution at the time when the average of the x -component of \mathbf{M} first crosses zero is shown in Figure 4.9. It matches well with the general expected behavior based on the results reported for example at [22].

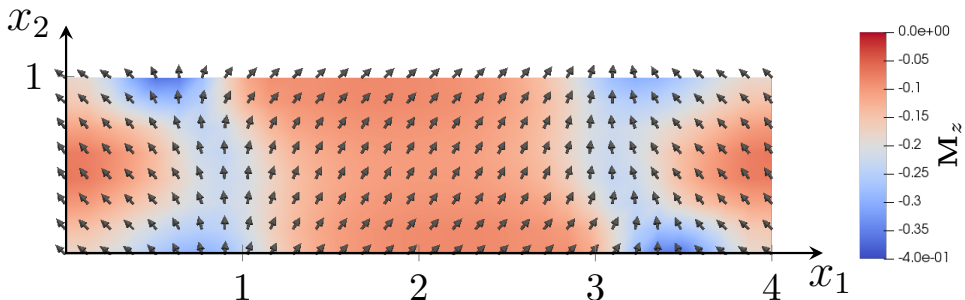


Fig. 4.9: HMM solution when the average of the x -component, $\langle M_x \rangle$, first crosses zero. Domain colored according to z -component of the magnetization.

5. Conclusion and outlook

In this article, we presented a Heterogeneous Multiscale Method for the Landau-Lifshitz equation with an oscillatory material coefficient which combines a finite element macro model with a finite difference micro problem based on results from [20]. Numerical

examples show the viability of the approach. It is thus possible to treat scale-separated problems with arbitrarily small variations ε , given a certain structure of those variations, such as local periodicity.

The current model includes the contributions of exchange interaction, applied external field and demagnetization to the effective field. However, in the given implementation, the demagnetization can only be computed for rectangular domains. This should be adjusted by using a different approach for solving the demagnetization problem in the future. Moreover, it would be interesting to study how to also include anisotropy effects into the model.

To keep focus on the multiscale aspect of the problem and for reasons of simplicity, we in this article chose a weak formulation for the macro model that does not specifically comply with the orthogonality structure given for the continuous problem. It should be rather simple to combine the proposed approach with schemes designed to take this into account such as explicit-in-time versions of [4, 7, 8]. Possible effects of doing so could be studied in the future.

A further interesting direction for future research could be to investigate whether it is possible to extend basis-representation techniques that have been proposed for HMM for linear problems, for example in [15], to the given Landau-Lifshitz problem. This could drastically reduce the number of micro problems that have to be solved and hence computational cost.

Acknowledgments. The authors would like to thank Prof. Olof Runborg and Prof. Gunilla Kreiss for many useful discussions along this work.

REFERENCES

- [1] ABDULLE, A., E, W., ENGQUIST, B., AND VANDEN-EIJNDEN, E. The Heterogeneous Multiscale Method. *Acta Numerica* 21 (2012), 1–87.
- [2] ABERT, C., BRUCKNER, F., VOGLER, C., WINDL, R., THANHOFFER, R., AND SUESS, D. A full-fledged micromagnetic code in less than 70 lines of numpy. *arXiv preprint arXiv:1411.7188* (2014).
- [3] ABERT, C., EXL, L., SELKE, G., DREWS, A., AND SCHREFL, T. Numerical methods for the stray-field calculation: A comparison of recently developed algorithms. *Journal of Magnetism and Magnetic Materials* 326 (2013), 176–185.
- [4] ALOUGES, F. A new finite element scheme for Landau-Lifshitz equations. *Discrete & Continuous Dynamical Systems-S* 1, 2 (2008), 187.
- [5] ALOUGES, F., DE BOUARD, A., MERLET, B., AND NICOLAS, L. Stochastic homogenization of the Landau-Lifshitz-Gilbert equation. *Stochastics and Partial Differential Equations: Analysis and Computations* (2021), 1–30.
- [6] ALOUGES, F., AND DI FRATTA, G. Homogenization of composite ferromagnetic materials. *Proceedings of the Royal Society A: Mathematical, Physical and Engineering Sciences* 471, 2182 (2015), 20150365.
- [7] ALOUGES, F., AND JAISSON, P. Convergence of a finite element discretization for the Landau-Lifshitz equations in micromagnetism. *Mathematical Models and Methods in Applied Sciences* 16, 02 (2006), 299–316.
- [8] ALOUGES, F., KRITSIKIS, E., STEINER, J., AND TOUSSAINT, J.-C. A convergent and precise finite element scheme for Landau-Lifshitz-Gilbert equation. *Numerische Mathematik* 128, 3 (2014), 407–430.
- [9] ARJMAND, D., AND RUNBORG, O. Analysis of heterogeneous multiscale methods for long time wave propagation problems. *Multiscale Modeling & Simulation* 12, 3 (2014), 1135–1166.
- [10] BARTELS, S., AND PROHL, A. Convergence of an implicit finite element method for the Landau-Lifshitz-gilbert equation. *SIAM journal on numerical analysis* 44, 4 (2006), 1405–1419.
- [11] CHAVES-O’FLYNN, G. D., KENT, A. D., AND STEIN, D. L. Micromagnetic study of magnetization reversal in ferromagnetic nanorings. *Physical Review B* 79, 18 (2009), 184421.

- [12] CHOQUET, C., MOUMNI, M., AND TILIOUA, M. Homogenization of the Landau-Lifshitz-Gilbert equation in a contrasted composite medium. *Discrete & Continuous Dynamical Systems-S* 11, 1 (2018), 35.
- [13] E, W., ENGQUIST, B., ET AL. The Heterogeneous Multiscale Methods. *Communications in Mathematical Sciences* 1, 1 (2003), 87–132.
- [14] E, W., ENGQUIST, B., LI, X., REN, W., AND VANDEN-ELJNDEN, E. Heterogeneous Multiscale Methods: a review. *Communications in computational physics* 2, 3 (2007), 367–450.
- [15] ENGQUIST, B., HOLST, H., AND RUNBORG, O. Multi-scale methods for wave propagation in heterogeneous media. *arXiv preprint arXiv:0911.2638* (2009).
- [16] ENGQUIST, B., AND TSAI, Y.-H. Heterogeneous Multiscale Methods for stiff ordinary differential equations. *Mathematics of computation* 74, 252 (2005), 1707–1742.
- [17] GEUZAIN, C., AND REMACLE, J.-F. Gmsh: A 3-D finite element mesh generator with built-in pre-and post-processing facilities. *International journal for numerical methods in engineering* 79, 11 (2009), 1309–1331.
- [18] LEITENMAIER, L., AND RUNBORG, O. On homogenization of the Landau-Lifshitz equation with rapidly oscillating material coefficient. *preprint, arXiv:2012.12567* (2020).
- [19] LEITENMAIER, L., AND RUNBORG, O. Heterogeneous Multiscale Methods for the Landau-Lifshitz equation. *arXiv preprint, arXiv:2108.09463* (2021).
- [20] LEITENMAIER, L., AND RUNBORG, O. Upscaling errors in heterogeneous multiscale models for the Landau-Lifshitz equation. *preprint, arXiv:2104.03206* (2021).
- [21] LOGG, A., MARDAL, K.-A., AND WELLS, G. *Automated solution of differential equations by the finite element method: The FEniCS book*, vol. 84. Springer Science & Business Media, 2012.
- [22] MICROMAGNETIC MODELING ACTIVITY GROUP (μ MAG), NIST CENTER FOR THEORETICAL AND COMPUTATIONAL MATERIALS SCIENCE (CTCMS). μ MAG standard problem #4. <https://www.ctcms.nist.gov/~rdm/mumag.org.html>.
- [23] NEWELL, A. J., WILLIAMS, W., AND DUNLOP, D. J. A generalization of the demagnetizing tensor for nonuniform magnetization. *Journal of Geophysical Research: Solid Earth* 98, B6 (1993), 9551–9555.
- [24] SANTUGINI-REPIQUET, K. Homogenization of ferromagnetic multilayers in the presence of surface energies. *ESAIM: Control, Optimisation and Calculus of Variations* 13, 2 (2007), 305–330.
- [25] SERPICO, C., MAYERGOYZ, I., AND BERTOTTI, G. Numerical technique for integration of the Landau-Lifshitz equation. *Journal of Applied Physics* 89, 11 (2001), 6991–6993.